Fusion of ^{58,60,62}Ni with 113–170 MeV ^{40}Ca ions

B. Sikora
Institute of Nuclear Physics, Warsaw University, Warsaw, Poland

J. Bisplinghoff
ISKP, Bonn University, Bonn, West Germany

W. Scobel
I. Institut für Experimentalphysik, Hamburg University, Hamburg, West Germany

M. Beckerman*
NSRL, University of Rochester, Rochester, New York 14627

M. Blann
NSRL, University of Rochester, Rochester, New York 14627
and E-Division, Lawrence Livermore Laboratory, Livermore, California 94550 †

(Received 30 May 1979)

Results of measurements of the fusion excitation functions of ^{58,60,62}Ni targets with 113–170 MeV (lab) ^{40}Ca ions are reported. These results are used to extract fusion barrier heights and radii by several different methods. Subbarrier fusion cross sections are analyzed in terms of static deformations. Possible importance of dynamic deformation is discussed. Conclusions as to the role of static deformation are similar to those from the ^{35}Cl + ^{58,60,62}Ni fusion system; a large part of the subbarrier behavior can be attributed to this cause.

[NUCLEAR REACTIONS ^{52,58}Ni (^{40}Ca, fusion), E_{Ca} = 113–170 MeV lab, measured evaporation residue excitation functions.]

I. INTRODUCTION

This work is the extension of a program of comprehensive measurements and interpretation of heavy ion induced fusion excitation functions.[1-7] The goal of the program is and has been the extraction of information on the potential-energy surface for deeply penetrating heavy ion reactions and of indications of dynamic and static effects on these potential surfaces.

Past measurements have provided reasonably precise results of fusion (evaporation residue plus fission or fissionlike) excitation functions for ^{32}S and ^{35}Cl projectiles on targets between ^{24}Mg and ^{141}Pr. In this work we present measurements involving the heavier and spherical projectile ^{40}Ca on ^{58,62}Ni targets. Special emphasis has been placed on measurements of fusion at near barrier energies in the hope of gaining insight into dynamic effects of the fusion barrier and the importance of static deformation. It is difficult to separate these two effects; however, comparison of the ^{40}Ca+Ni data with corresponding ^{35}Cl+Ni results (in the sudden approximation approach) may allow differentiation between target and projectile static deformation contributions.

There is some question as to how to extract fusion barriers and radii from data of this type. We will explore several methods, pointing out some pitfalls of one and discussing limitations on the classical method of analysis. The barrier values extracted will be compared with predictions of the proximity potential.[8]

II. EXPERIMENTAL PROCEDURE AND RESULTS

The ^{40}Ca beam was from the Rochester MP tandem Van de Graaff accelerator. Isotopically enriched targets of ^{58,60,62}Ni were used, self-supporting or on 5 μg/cm^2 carbon backings ranging from 50 to 147 μg/cm^2 thick and with less than 0.1% contamination of the heavier nickel isotopes. These targets were bombarded with ^{40}Ca ions with lab energies between 113 and 176 MeV, energy determinations being based on analyzing magnets. The average center-of-mass energies given in Table I are corrected for loss of projectile energy in the target, taking into account the slope of the excitation functions $\sigma_{ER}(E)$.

The evaporation residues (ER), as well as the elastically scattered Ca ions, Ni recoils, and transfer-reaction products, were detected by two telescopes, each consisting of a ΔE proportional counter and a $(E - \Delta E)$ solid state detector.[1] Beam position on target, beam intensity, and target intensity, and target thickness were monitored by

two solid state counters mounted symmetrically at ±17° with respect to the beam axis. The detector angle was thus defined to better than 0.2°. The total acceptance angle was 0.9°, taking into account the beam size on target and the detector aperture (1×4 mm; at forward angles a 1 mm circular tantalum aperture was used). Further details of the experimental technique are given in Refs. 1 and 3.

Data were taken between 2.3° and 15° (lab) in 1 or 2° steps. The absolute differential cross sections for evaporation residues were derived by normalizing the relative cross sections to the simultaneously measured elastic scattering which, in this angular region, is purely determined by Rutherford

TABLE I. Summary of cross sections obtained in this study. Critical angular momenta l_{cr} are derived from $\sigma_{CF} = \sigma_{ER} + \sigma_{FISS}$ in the sharp cutoff model.

Reaction	$E_{c.m.}$ (MeV)	σ_{ER} (mb)	$\Delta\sigma_{ER}$ (%)	σ_{FISS} (mb)	l_{cr} (σ_{CF})[a]
$^{40}Ca + ^{58}Ni$	68.1	0.6	50		0.2
	69.4	3.2	50		1.8
	70.7	14	18		5.0
	72.5	47	10		10
	73.7	71	10		13
	74.9	95	10		15
	76.7	152	10		20
	78.4	201	10		23
	80.8	276	10		27
	85.5	451	10		36
		429	10		
	94.4	637	10		46
	97.4	653	10		(47)[c]
$^{40}Ca + ^{60}Ni$	68.2	3.1	35		1.8
	69.1	10	40		4.1
	69.4	10.3	15		
	70.6	24.7	10		7.0
	71.7	49.8	11		10.4
	86.6	507	12		39
$^{40}Ca + ^{62}Ni$	68.3	6.8	16		1.0
	68.9	13.2	15		4.8
	69.2	14.0	20		5.0
	70.0	30	20		7.6
	70.1	27.5	15		
	71.3	50.0	20		11
		49.2	10		
		56.6	10		
	72.5	77.2	10		14
		82	20		
	74.3	136	10		18
	75.6	172	10		21
	76.8	213	10		24
	78.6	265	10		27
	80.4	350	10		31
	82.9	392	10		34
	84.6	502	10		39
	87.6	606	10		43
	87.7	615	10		
	90.6	607	10		44
	93.7	685	10		48
	96.8	732	10	20 ± 10	51
	99.8	761	10	40[d]	53
	99.9	737	10	40[d]	
	102.9	787	10	60 ± 20	56
	106.7	940	15		(60)[c]

[a] From $\sigma_{CF} = \pi\lambda^2(l_{cr}+1)^2$.
[b] Average value has been used in the analysis.
[c] Excluded from σ_{CF} analysis.
[d] Interpolated.

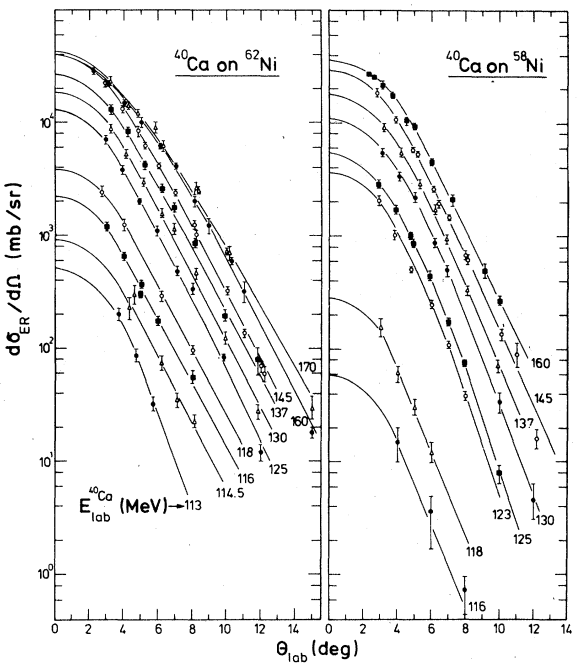

FIG. 1. Angular distributions of the evaporation residues at various energies for the systems ^{40}Ca + ^{58,62}Ni. Intergrations were performed over the smoothed distributions (solid lines).

scattering. At angles below 6°, the monitor counters were used with Rutherford normalizations from larger angles to get absolute cross sections. In Fig. 1, a representative set of angular distributions for the evaporation residue cross sections is shown for the reactions ^{40}Ca on ^{58,62}Ni at various energies. Integration over angle yields the total evaporation residue cross section. The extrapolation of the data into the 0–3° region sets the lower limit in the absolute error to 7–10%. Well above the barrier, the relative errors in the fusion excitation functions are only about 5% due to the similar shapes of the angular distributions; at the lowest projectile energies they reach 50% due to the poorer statistics and the influence of target contaminations.

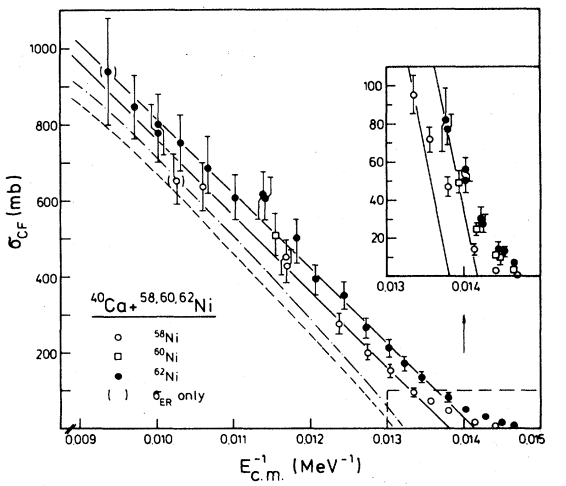

FIG. 2. Excitation function of complete fusion for ^{40}Ca on ^{58,60,62}Ni as a function of $E_{c.m.}^{-1}$. The straight lines are the result of Eq. (1) with the parameters given in Table III. The proximity potential calculation including proximity friction (Ref. 11) is given for ^{58}Ni (dashed line) and for ^{62}Ni (dashed-dotted line).

The resulting evaporation residue cross sections can be interpreted as complete fusion cross sections for projectile energies up to 160 MeV. At 160 and 170 MeV, measurements were performed with one telescope shifted to angles θ_{lab} between 15° and 35°. The observed fissionlike events were used to derive an upper limit for fission following fusion by assuming the $1/\sin\theta_{c.m.}$ distribution of symmetric binary fission from an equilibrated system. The resulting data are presented in Table I, and in Fig. 2 as a function of $\epsilon_{c.m.}^{-1}$.

III. INTERPRETATION OF DATA

A. General comments

We have analyzed much of our past fusion excitation function data by the classical relationship[1,3-6]

$$\sigma_{fus}(\epsilon_{c.m.}) = \pi R_0^2 (1 - V_0/\epsilon_{c.m.}) . \quad (1)$$

Analysis is performed by fitting Eq. (1) to experimental fusion cross sections to extract R_0 and V_0. As has been pointed out previously,[1,4,6] the assumptions implicit in Eq. (1) are as follows:

(1) There is a minimum distance R_0 and potential height V_0 which target and projectile must have in order to fuse.

(2) Forces are conservative; all energy is in relative kinetic or potential energy of the target-projectile pair.

(3) All particle trajectories fulfilling condition (1) will lead to fusion.

Our application of Eq. (1) has been restricted to the region of the excitation function sufficiently above the energy where barrier penetrability is significant, and below energies where we observe large contributions from deep inelastic processes. This provides a fairly broad energy range over which our data points do give a linear relationship when plotted versus $1/\epsilon_{c.m.}$. This is a necessary, though not necessarily sufficient, condition for application of Eq. (1).

Some attention has been given to the effects which energy dissipation might have in modifying the usefulness of Eq. (1) in extracting fusion parameters. Model calculations in which some degree of dissipation was explicitly included seem to give results

TABLE II. Two and three parameter fit results of Eqs. (1) and (3) to experimental complete fusion data.

Reaction	No. of points	R_0 (fm)	V_0 (MeV)	$\hbar\omega_0$ (MeV)	χ^2	E/V_0 [a]
$^{40}Ca + ^{58}Ni$	12	8.92 ± 0.21	71.66 ± 0.22	6.07 ± 0.49	1.15	0.950–1.317
	10	9.33 ± 0.29	72.38 ± 0.42	9.39 ± 0.75	0.61	0.986–1.317
	7	9.60 ± 0.47	72.96 ± 0.96	11.2 ± 6.9	0.21	1.045–1.317
$^{40}Ca + ^{62}Ni$	19	9.41 ± 0.16	70.70 ± 0.26	8.29 ± 0.71	0.47	0.965–1.455
	18	9.46 ± 0.17	70.83 ± 0.29	8.98 ± 0.95	0.42	0.974–1.455
	14	9.52 ± 0.22	71.01 ± 0.51	10.0 ± 4.1	0.46	1.026–1.455
$^{35}Cl + ^{58}Ni$	b	9.00 ± 0.21	61.3 ± 0.3	5.0 ± 1.0	1.13	0.98–1.42
$^{35}Cl + ^{62}Ni$	b	9.60 ± 0.21	60.8 ± 0.3	8.4 ± 1.0	0.20	0.97–1.46
$^{40}Ca + ^{58}Ni$	7	9.4 ± 0.3	72.4 ± 0.3	...	0.28	1.045–1.317
$^{40}Ca + ^{62}Ni$	14	9.4 ± 0.2	70.6 ± 0.2	...	0.54	1.026–1.317

[a] Referring to $V_0 = 71.7$ (70.7) MeV for ^{58}Ni (^{62}Ni).
[b] Reference 3.

similar to those of Eq. (1) for the systems which we have investigated.[9,10] It has also been suggested that a better analysis of the data results from using, e.g., the proximity nuclear potential plus Coulomb and centrifugal potential and finding V_0 and R_0 for s waves by fitting calculated cross sections to experimental results.[11] This is done under the assumption that all partial waves for which the one-dimensional potential shows a maximum will lead to fusion—or in more complicated calculations, those trapped in the pockets by energy dissipation. We will, in subsequent analyses, point out some difficulties and errors which may arise from this method of analysis.

It should be emphasized that the assumption (1) is a gross approximation in that it assumes R_0 and V_0 are static properties independent of bombarding energy. Analyses fitting to one-dimensional potentials do allow for a change in R_0 due to an assumed form of centrifugal potential. But they do not recognize that V_0 is not a true saddle point barrier, nor that the fusion process involves other degrees of freedom than are included in the one-dimensional treatment. The neck formation process is probably of primary importance and we will discuss this point subsequently. The dynamics of neck formation could, of course, alter the radial position required for fusion from that required by a one-dimensional potential. It may then turn out that simple analysis of data by Eq. (1), with recognition of uncertainties in the parameters extracted, is the method of choice when the data are linear versus $1/\epsilon_{c.m.}$.

B. Data analyses with barrier penetrability

Applying the Wong ansatz[12]

$$\sigma_{CF}(\epsilon_{c.m.}) = \frac{R_0\hbar\omega_0}{2\epsilon} \ln\left|1+\exp\left[2\pi\left(\frac{\epsilon_{c.m.}-V_0}{\hbar\omega_0}\right)\right]\right| \quad (2)$$

to our data by searching for the best fitting parameters R_0, $\hbar\omega_0$, and V_0, we find different results, depending on the lowest projectile energy included in the search (Table II).

If we first look at the fits to the complete data sets, we can state the following:

(a) The radius parameter R_0 turns out to be on the order of 0.5 fm larger for $^{40}Ca + ^{62}Ni$ than for $^{40}Ca + ^{58}Ni$. This is more than what is expected from an $R \sim (A_p^{1/3} + A_T^{1/3})$ dependence.

(b) The barrier V_0 is about 1 MeV higher for the $^{58}Ni + ^{40}Ca$ system than that of $^{62}Ni + ^{40}Ca$.

(c) The curvature $\hbar\omega_0$ is more than 2 MeV smaller for the reaction with ^{58}Ni, i.e., the excitation function $\sigma_{CF}(E)$ falls off more steeply with decreasing energy as is the case for $^{40}Ca + ^{62}Ni$.

These observations (a)–(c) show a remarkable agreement with the trends emerging from the corresponding data obtained for ^{35}Cl induced fusion with $^{58,62}Ni$[3] (Table II). The absolute values of the fusion radii for ^{40}Ca induced fusion are slightly smaller than when extrapolated from the ^{35}Cl data, assuming an $A^{1/3}$ dependence. The same holds for the barriers if compared on a $V_0 \sim Z_P Z_T$ basis.

One should, however, use these differences only as indicators for inconsistencies and not stress the physical interpretation of these parameters, for it should be remembered that Eq. (2), when applied far in the sub-barrier region, is only a crude approximation.[13,14] This may be seen by comparing the fitted parameters obtained by stepwise reduction of the data sets by the low energy points (Table II). Under this procedure, the parameters V_0 and R_0 are systematically increased for ^{58}Ni targets, indicating that at low energies the deviation of the experimental data from the classical $1/\epsilon_{c.m.}$ dependence is insufficiently described by the penetrability through an inverted parabola of curva-

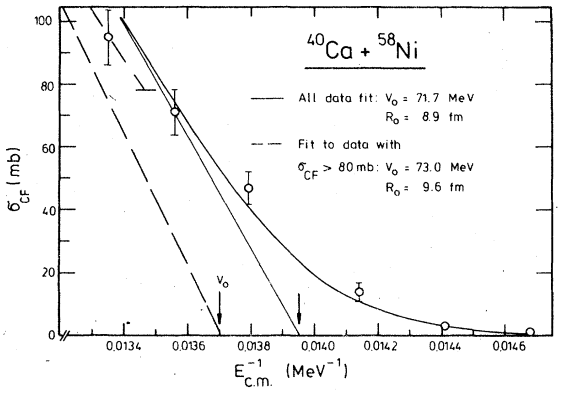

FIG. 3. Dependence on the best fit parameters V_0 and R_0 [Eq. (2)] on the sub-barrier part of the excitation function. The straight lines (solid and dashed) are calculated by inserting R_0 and V_0 into Eq. (1).

ture $\hbar\omega_0$. In the fitting procedure, the deviation is therefore minimized by lowering the barrier height V_0, accompanied by a reduction of the independent variable R_0 to account for a good fit at higher energies (see Fig. 3). In the fits with the smallest number of low energy points, the error in $\hbar\omega_0$ is substantially increased due to the insensitivity of the data to $\hbar\omega_0$.

Are these shortcomings due to the fact that Eq. (2) cannot be applied in the sub-barrier region? Probably not, as may be seen from Fig. 4. At small distances (i.e., inside the potential pocket) the potential consisting of a nuclear and a Coulomb part is reasonably reproduced by the parabolic fit,

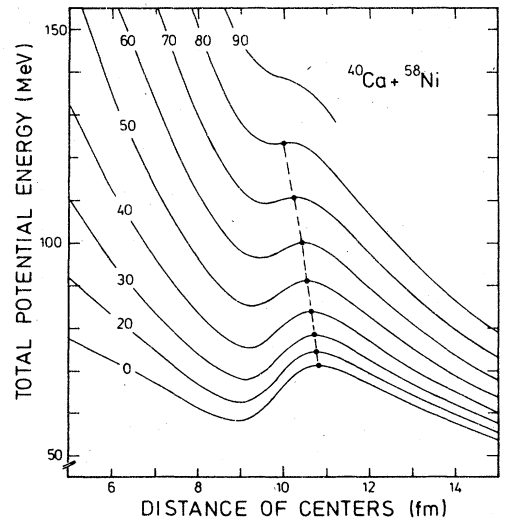

FIG. 4. Total real potential $V(r) = V_N(r) + V_l(r)$ for different angular momenta. The nuclear contribution is calculated from an optical model potential with Woods-Saxon form factor (see text). The solid points indicate the barrier positions.

whereas far out the Coulomb part takes over and the barrier becomes systematically broader than described by the parabolic approximation. Therefore, in the sub-barrier region the parabolic model is likely to produce cross sections too *high*,[13] resulting in a compensating *increase* of the fitted parameters V_0 and R_0. This is just opposite to the trend we observe. We must then conclude that other effects so far not taken into consideration modify the excitation functions $\sigma_{CF}(E)$ and cause a slower descent at low energies. Among possible effects to consider are the following:

(i) Experimental reasons: insufficient energy resolution, e.g., due to thick targets, background effects (recoiling target nuclei and elastic scattering or transfer reactions and products from reactions with carbon deposited on the target);

(ii) Ground state quadrupole deformations of projectile and/or target nucleus causing barriers of different heights for different relative orientations between target and projectile nucleus.[3,12,14-17]

(iii) Dynamic deformations of the nuclei undergoing fusion. The neck forms and broadens during the collision, enhancing the penetrability by reducing the barrier height; in addition, sub-barrier resonances due to quantal zero-point oscillations are predicted to occur.[18]

For our data, the average energy E was determined, taking the target thickness into account, by calculating the average with a weighting proportional to $\sigma_{CF}(E)$. Inspection of kinematics shows that for Q values up to -30 MeV the kinetic energies of the targets and targetlike recoils differ, at least, by a factor of 2 from the evaporation residue energies. Contributions from carbon deposits and backing have been accounted for by background runs. Regarding (ii), this effect is usually taken into account by averaging over orientation[3,12] or by averaging transmission coefficients of potential barriers being uniformly distributed over an interval ΔE centerd at V_0.[16] Typical values of ΔE are 3–4 MeV. In this procedure, however, a slight reduction of V_0 significantly reduces the size of ΔE. On the other hand, this would lead to an overestimate of σ_{CF} above the barrier and would require a mechanism competing with fusion[11] for partial waves passing above the fusion barrier. Measurements for ^{40}Ca + ^{62}Ni at E_{lab} = 160 and 170 MeV performed near the grazing angle showed no appreciable deep inelastic component which might qualify.

The inclusion of (ii) and (iii) can be made with different approaches. If one assumes that both effects produce penetrabilities equivalent to a uniform spectrum ΔE of barrier heights, an averaging over ΔE can be applied. As long as dynamical effects are small (e.g., for light nuclei[19]) one may

TABLE III. Three parameter fit results of Eq. (2) to experimental complete fusion data.

Reaction	β_2^{Ca}	β_2^{Ni}	R_0 (fm)	V_0 (MeV)	$\hbar\omega_0$ (MeV)	χ^2
$^{40}Ca+^{58}Ni$	0 [a]	0 [a]	8.92	71.7	6.1	1.15
	0 [a]	−0.2 [a,b]	9.04	72.3	4.3	0.60
	0 [a]	−0.23 [b]	9.22	72.8	4.5 [a]	0.56
$^{40}Ca+^{62}Ni$	0 [a]	0	9.41	70.7	8.3	0.47
	0 [a]	−0.2 [a]	9.42	71.7	6.5	0.43
	0 [a]	−0.28	9.45	71.7	4.5 [a]	0.38

[a] These parameters were kept fixed.
[b] No reasonable fits obtained for $\beta_2^{Ni} > 0$.

try to take into account only static quadrupole deformations β_2 and follow the suggestion of Wong[12] to average Eq. (1) over orientations yielding

$$\langle \sigma_{CF}(E) \rangle = \frac{1}{16\pi^2} \oint\oint \sigma_{CF}(E, \theta_1, \theta_2) d\Omega(\theta_1) d\Omega(\theta_2), \quad (3)$$

with the angles θ_2 measured between the collision axis and the symmetry axis of the ith nucleus. As both parameters $\hbar\omega_0$ and β_2^{Ni} change the excitation function in a similar way, it seems unreasonable to search for both simultaneously. Therefore, Table III contains only three parameter best fits to the complete excitation functions where either $\hbar\omega_0$ or β_2^{Ni} was kept fixed; for $\hbar\omega_0$ a value of 4.5 MeV was then chosen.[11,13] For β_2^{Ni} values obtained from experimental $B(E2, 0^+ \rightarrow 2^+)$ transition probabilities in the rigid spheroidal rotor model were taken[20] (see, however, Ref. 3). The projectile was assumed to be spherical.

The inclusion of static deformations in this way, in spite of its shortcomings,[21] improves the overall quality of fits. However, in view of the very large increases of penetrability to be expected from neck formation, the latter dynamical effect may well turn out to be the more important explanation for the near and sub-barrier behavior of the fusion excitation functions. Kodama *et al.*[18] have shown that, for the symmetric system $^{100}Mo+^{100}Mo$, the penetrability for a two-dimensional potential-energy surface $V(r, \sigma)$, depending on the center-of-mass separation r and a fragment elongation coordinate σ, is substantially higher below V_0 than that for a corresponding one-dimensional parabolic barrier. Whereas this tendency is expected for our asymmetric system $^{40}Ca+Ni$, too, no calculation could be performed[22] because the mass asymmetry introduces a third degree of freedom.

In order to exclude the inherent uncertainties of the barrier region in the determination of the barrier parameters V_0 and R_0, we restrict the analysis to the $1/\epsilon_{c.m.}$ region and reduce Eq. (2) to Eq. (1). The results of the two parameter best fits are given in Table II. It is seen that for this region no significant difference in the radial position R_0 can be stated, whereas the fusion barrier heights seem to be slightly higher for ^{58}Ni than for ^{62}Ni. This may imply a smaller radius for ^{58}Ni. A similar conclusion was reached for the fusion of $^{16,17,18}O$ with ^{12}C.[19] The R_0 and V_0 parameters deduced by Eq. (1) are consistent with those deduced with Eq. (2) for ^{62}Ni, but not for ^{58}Ni when a large proportion of sub-barrier points is included in the analysis.

We next address the question of the adequacy of using Eqs. (1) or (2) with the assumption that $\hbar\omega_l = \hbar\omega_0$, $R_l = R_0$, and $V_l = V_0 + \hbar^2 l(l+1)/2\mu R_0^2$. In order to illuminate the l dependence of the barrier curvature and of the fusion radius, one may calculate $V(r)$ as a sum of the Coulomb potential of a homogeneously charged sphere and a nuclear part. For the latter we have chosen the following:

(i) The real part of the optical model potential[23] describing the elastic scattering of $^{40}Ca+^{40}Ca$. It is of Woods-Saxon shape ($V = 35$ MeV; $r_0 = r_{0c} = 1.35$ fm, $a = 0.43$ fm). This is a fairly shallow nuclear potential providing an upper limit of the l dependence as far as this static effect is concerned.

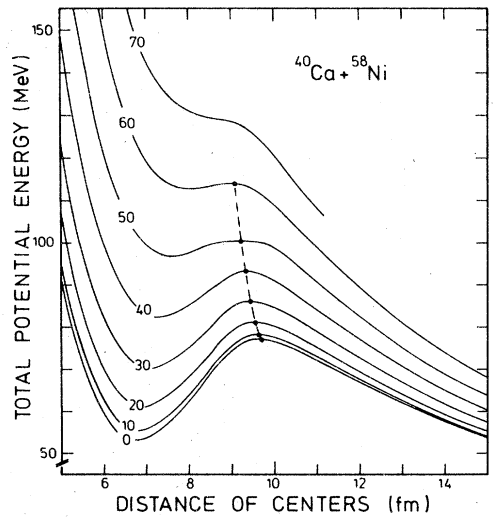

FIG. 5. Same as Fig. 4, with V_N calculated from Blocki's proximity potential (Ref. 8) (see text).

TABLE IV. Experimental and calculated barrier parameters.

System	R_{fus} (expt)[a]	V_{fus} (expt)[a]	V_n (expt)	Proximity potential V_n (R_{expt})1	Proximity potential R_{fus}	Proximity potential V_{fus}[a]	Proximity potential V_n
^{40}Ca + ^{58}Ni	9.6 ± 0.3	73.0	−11.0	−11.0	9.8	75.7	−5.6
^{40}Ca + ^{62}Ni	9.5 ± 0.2	71.0	−13.6	−10.2	9.9	75.2	−6.3

[a] See Table II.
[b] Calculated at R_{fus} from proximity potential.

Within the region of l values covered in this work (l=0–50), R_l decreases from 10.8 to 10.55 fm and $\hbar\omega$ increases from 4.87 MeV for s waves to 5.94 MeV. A graphic presentation is given in Fig. 4.

(ii) The proximity potential which has been successfully applied to the analysis of fusion excitation functions.[10] In the energy region under consideration the friction may be neglected.[9] The proximity potential has been taken from Blocki *et al.*[8]:

$$V_N(\xi)=4\pi\gamma b\,\frac{C_P C_T}{C_P+C_T}\,\phi(\xi),$$

where the surface energy coefficient γ (in MeV/fm^2) is

$$\gamma=0.9517\left|1-1.7826\left(\frac{N_{CN}-Z_{CN}}{A_{CN}}\right)^2\right|;$$

the central radius

$$C=R\left|1-(b/R)^2+\cdots\right|$$

is related to the effective sharp radius R (in fm)

$$R=1.28A^{1/3}-0.76+0.8A^{-1/3} \qquad (4)$$

and to the width b which has been given the approximate value of 1 fm. The universal function $\phi(\xi)$ of the separation in units of b, $\xi=(r-C_P-C_T)/b$ has been approximated[8] by

$$\phi(\xi)=-0.5(\xi-2.54)^2-0.0852(\xi-2.54)^3$$
$$\text{for } \xi\leq 1.2511$$
$$=-3.437\exp(-\xi/0.75) \quad \text{for } \xi\geq 1.2511.$$

The resulting potential barriers are shown in Fig. 5. Within the interval l=0–50, the barrier position R_l decreases from 9.64 fm to 9.22 fm, and the curvature $\hbar\omega_0$ increases from 4.15 MeV to 5.37 MeV.

We may conclude that the results for R_0 and V_0 given in Tables II and III are within the quoted uncertainties for effects due to neglect of the related dependence of R_l. This is not generally the case for systems of nuclei undergoing fusion and Eq. (1) must be applied with consideration of this point.

The radii and barriers given in Table II may be converted to values of the nuclear potential at R_0 by subtracting the Coulomb potential from the barrier V_0. This is done in Table IV for the R_0 and V_0 results extracted using Eq. (2) to analyze the fusion data. Also included are the nuclear potentials predicted by the proximity potential at the same value of R_0. The last three columns of Table IV give the fusion radius, R_{fus}, barrier height V_{fus}, and nuclear contribution V_N predicted *a priori* by the proximity potential. These results give a radius close to R_0, too low a nuclear interaction and too high a barrier. Accordingly, the excitation functions $\sigma_{CF}(1/\epsilon_{c.m.})$, calculated with the proximity potential and the proximity one-body nuclear friction, underestimate the experimental results but show the correct slope (cf. Fig. 2). The discrepancy can be reduced by a readjustment of the nuclear matter radii R^{11} in Eq. (4). In the case of ^{35}Cl+Ni, a shift of ΔR=0.16 fm was sufficient.[9] The same value ΔR is necessary to obtain good overall agreement for ^{40}Ca+^{58,62}Ni; it results in an increase of R_{fus} by 0.4 fm and a decrease of V_{fus} by 3.1 MeV.

IV. CONCLUSION

For the systems presented in this work, the fusion data indicate a linear relationship on a cross section versus $1/\epsilon_{c.m.}$ plot. Analysis by the classical formula,[1] which assumes the existence of a fusion barrier, gives parameters consistent with those extracted by the formula due to Wong, which includes barrier penetrability effects, if the latter analysis does not contain too large a percentage of near and sub-barrier points. When many sub-barrier points are included in the analysis, distorted values of R_0 and V_0 result from the fitting process. The low energy fitting can be improved by including a spread in barrier heights due to static target deformations. However, it is probable that dynamic deformations such as necking effects are important in determining the penetrability at low energies. The proximity potential gives reasonable agreement for the nuclear potential at the radius deduced from $1/\epsilon_{c.m.}$ analysis, perhaps slightly less deep, consistent with earlier conclusions[5] based on the similar potential of Ngô *et al.*[24]

The authors are grateful to Dr. J. Birkelund for the calculation of the fusion excitation functions with the proximity potential.

*Permanent address: Laboratory for Nuclear Science, MIT, Cambridge, Mass.
†Permanent address.

[1]H. H. Gutbrod, W. G. Winn, and M. Blann, Nucl. Phys. A213, 267 (1973).
[2]H. H. Gutbrod, M. Blann, and W. G. Winn, Nucl. Phys. A213, 285 (1973).
[3]W. Scobel, A. Mignerey, M. Blann, and H. H. Gutbrod, Phys. Rev. C 11, 1701 (1975).
[4]H. C. Britt, B. H. Erkkila, R.H. Stokes, H. H. Gutbrod, F. Plasil, R. L. Ferguson, and M. Blann, Phys. Rev. C 13, 1483 (1976).
[5]W. Scobel, H. H. Gutbrod, M. Blann, and A. Mignerey, Phys. Rev. C 14, 1808 (1976).
[6]P. David, J. Bisplinghoff, M. Blann, T. Mayer-Kuckuk, and A. Mignerey, Nucl. Phys. A287, 179 (1977).
[7]J. Bisplinghoff, P. David, M. Blann, W. Scobel, T. Mayer-Kuckuk, J. Ernst, and A. Mignerey, Phys. Rev. C 17, 177 (1978).
[8]J. Blocki, J. Randrup, W. J. Swiatecki, and C. F. Tsang, Ann. Phys. (N.Y.) 105, 427 (1977).
[9]J. R. Birkelund, J. R. Huizenga, J. N. De, and D. Sperber, Phys. Rev. Lett. 17, 1123 (1978).
[10]J. R. Birkelund and J. R. Huizenga, Phys. Rev. C 17, 126 (1978).
[11]L. C. Vaz and J. M Alexander, Phys. Rev. C 18, 2152 (1978).
[12]C. Y. Wong, Phys. Rev. Lett. 31, 766 (1973).
[13]Y. Avishai, Z. Phys. A286, 285 (1978).
[14]H. Feiesleben and J. R. Huizenga, Nucl. Phys. A224, 503 (1974).
[15]H. J. Krappe and H. Massmann, Z. Phys. A286, 331 (1978).
[16]L. C. Vaz and J. M. Alexander, Phys. Rev. C 10, 464 (1974).
[17]J. M. Alexander, L. C. Vaz, and S. Y. Lin, Phys. Rev. Lett. 33, 1487 (1974).
[18]P. Kodama, R. A. M. S. Nazareth, P. Möller, and J. R. Nix, Phys. Rev. C 17, 111 (1978).
[19]Y. Eyal, M. Beckerman, R. Chechik, Z. Fraenkel, and H. Stocker, Phys. Rev. C 13, 1527 (1976).
[20]A. Christie and O. Häusser, Nucl. Data A11, 281 (1973).
[21]R. G. Stokstad, Y. Eisen, S. Kaplanis, D. Pelte, U. Smilanski, and I. Tserruya, Phys. Rev. Lett. 41, 465 (1978).
[22]P. Möller and J. R. Nix, private communication.
[23]H. Doubré, J. C. Jamart, E. Plagnol, N. Poffé, M. M. Riou, and J. C. Roynette, Phys. Rev. C 15, 693 (1977).
[24]C. Ngô, B. Tamain, M. Beiner, R. J. L. Lombard, D. Mas, and H. H. Deub, Nucl. Phys. A252, 237 (1975).